

Crystal growth, characterization, and phase transition of $\text{PbCuTe}_2\text{O}_6$

A. R. N. Hanna ^{1,2,*} A. T. M. N. Islam ² R. Feyerherm ² K. Siemensmeyer ² K. Karmakar,²
S. Chillal ^{2,†} and B. Lake ^{2,1}

¹*Institut für Festkörperphysik, Technische Universität Berlin, Hardenbergstrasse 36, 10623 Berlin, Germany*

²*Helmholtz-Zentrum Berlin für Materialien und Energie, Hahn-Meitner-Platz 1, 14109 Berlin, Germany*



(Received 2 August 2021; accepted 27 September 2021; published 2 November 2021)

Single crystals of the three-dimensional frustrated magnet and spin liquid candidate $\text{PbCuTe}_2\text{O}_6$ were grown using both the traveling solvent floating zone and the top-seeded solution growth (TSSG) techniques. The growth conditions were optimized by investigating the thermal properties. The quality of the crystals was checked by polarized optical microscopy, x-ray Laue, and x-ray powder diffraction and compared to the polycrystalline samples. Excellent quality crystals were obtained by the TSSG method. Magnetic measurements of these crystals revealed a small anisotropy for different crystallographic directions in comparison with the previously reported data. The heat capacity of both single-crystal and powder samples reveal a transition anomaly around 1 K. Curiously the position and magnitude of the transition are strongly dependent on the crystallite size, and it is almost absent for the smallest crystallites. A structural transition is suggested which accompanies the reported ferroelectric transition, and a scenario whereby it becomes energetically unfavorable in small crystallites is proposed.

DOI: [10.1103/PhysRevMaterials.5.113401](https://doi.org/10.1103/PhysRevMaterials.5.113401)

I. INTRODUCTION

Strongly correlated systems have a wide range of fascinating properties that explain and verify the existence of novel quantum phenomena. Among these systems, some lattice geometries introduce unique examples of highly frustrated magnetic systems with novel behavior, such as quantum spin liquids (QSLs) [1,2] and spin ice systems [3–6]. The QSL is an unusual magnetic ground state caused by the interaction of quantum spins in certain magnetic materials with highly frustrated or competing interactions. QSLs are associated with the absence of long-range magnetic order and exhibit fractionalized excitations due to the quantum entanglement [7].

$\text{PbCuTe}_2\text{O}_6$ (PCTO) is a rare example of a potential QSL hosted in a three-dimensional (3D) magnetic lattice known as the hyperhyperkagome [8]. This is a 3D network of corner shared triangles formed by the $S = 1/2$ Cu^{2+} spins (three triangles per spin) similar to, but distinctly different from the more well-known hyperkagome lattice (two triangles per spin). The Cu^{2+} spins in $\text{PbCuTe}_2\text{O}_6$ are coupled by various frustrated and nonfrustrated antiferromagnetic exchange interactions [9]. More detailed theoretical calculations suggest that the magnetic interactions extend to four nearest neighbors where the first and second nearest neighbors (J_1 , J_2) are equally strong and are involved in the frustrated hyperhyperkagome lattice whereas the third and fourth neighbors (J_3 , J_4) form unfrustrated antiferromagnetic chains [8]. Figure 1(a) explains the crystal structure of $\text{PbCuTe}_2\text{O}_6$ where the cubic structure (space-group $P4_132$, lattice constant = 12.49 Å at 300 K) is formed from CuO_4 square plaquettes, TeO_3 units, and Pb atoms. The arrangement of magnetic Cu^{2+} ($S = \frac{1}{2}$)

ions forming the hyperhyperkagome lattice is indicated in Fig. 1(b) by the red and blue lines.

The strong frustration of the system is revealed by the absence of any static long-range magnetic ordering in the magnetic susceptibility, heat capacity, muon spin relaxation, and neutron-diffraction measurements of the polycrystalline samples of PCTO down to 20 mK [8–10]. Although the heat capacity of the powder revealed a broad hump at $T \sim 1$ K and a weak anomaly at $T \sim 0.87$ K [9], a long-range magnetic ordering was ruled out due to the absence of a λ -like anomaly. Inelastic neutron scattering of a polycrystalline sample at ($T = 0.1$ K) revealed a diffuse nondispersive continuum of magnetic excitations, a feature suggestive of the fractionalized excitations [8]. The diffuse scattering forms spheres in reciprocal space as seen in the single-crystal samples [8], a 3D analog of the two-dimensional diffuse scattering rings observed in the kagome QSL Herbertsmithite and $\text{Ca}_{10}\text{Cr}_7\text{O}_{28}$ [11,12], hence, supporting the QSL interpretation of PCTO.

The crystal structure of PCTO and the experimental evidence for the absence of static magnetism have only been reported extensively in the polycrystalline samples. The information on structural and bulk properties of single crystals of PCTO remains inconclusive. For example, the submillimeter single crystals synthesized using the hydrothermal method report a larger lattice parameter (12.60 Å, $P4_332$) [13,14]. In addition, all single crystals also indicate a phase transition at $T \sim 1$ K [8,15]. Therefore, it is necessary to obtain large high-quality $\text{PbCuTe}_2\text{O}_6$ single crystals suitable for the investigation of thermodynamic and magnetic properties as well as eventually inelastic neutron-scattering measurements to study the possible QSL state.

$\text{PbCuTe}_2\text{O}_6$ is a relatively new compound of which very little is known about its temperature-composition phase equilibrium. The differential thermal analysis elucidated that $\text{PbCuTe}_2\text{O}_6$ has a high tendency toward incongruent melting;

*abanoub.hanna@helmholtz-berlin.de

†shravani.chillal@helmholtz-berlin.de

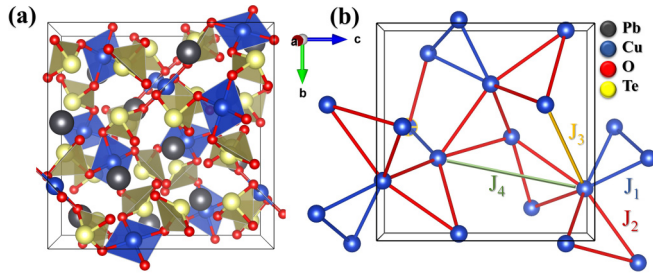


FIG. 1. (a) Visualization of the cubic structure of $\text{PbCuTe}_2\text{O}_6$ (space-group $P4_132$) indicating the distribution of CuO_4 square plaquettes, TeO_3 units, and Pb atoms where the Pb, Cu, Te, and O are colored gray, blue, yellow, and red, respectively. (b) The distribution of the Cu^{2+} ions inside the lattice forming a three-dimensional network of corner-shared triangles (hyperhyperkagome lattice). The first neighbor interactions (J_1 , blue lines) and the second-neighbor interactions (J_2 , red lines) have similar strengths [8,9], although the weaker third interactions (J_3 , orange line) and fourth interactions (J_4 , green line) form the antiferromagnetic chains [8].

our initial experiments revealed a decomposition at 600°C and the presence of the other phases Cu_3TeO_6 , $\text{Pb}_2\text{Te}_3\text{O}_8$ which are clear indications of the instability of the melt. Besides, due to its proximity to the crystalline phase $\text{PbCuTe}_2\text{O}_7$ [16] which has a slightly higher oxidation state, the growth atmosphere of $\text{PbCuTe}_2\text{O}_6$ needs to be optimized carefully. For these reasons, the growth of large and high-quality single crystals of $\text{PbCuTe}_2\text{O}_6$ is considered quite challenging. Among different crystal-growth techniques, the traveling solvent floating zone technique (TSFZ) is known for the successful growth of many such complex oxide compounds [17,18]. It provides high-purity crystals because of its advantage in controlling the growth atmosphere and the absence of contact of the melt with any other material (e.g., crucible, wires, covers, etc.). Many novel quantum magnets were grown using this technique, such as the quantum spin liquid candidate $\text{Ca}_{10}\text{Cr}_7\text{O}_{28}$ [12], CaCr_2O_4 with distorted triangular lattice [19] and the candidate quantum spin-ice system $\text{Pr}_2\text{Hf}_2\text{O}_7$ [20]. However, some compounds have very low surface tension in the molten form, and a stable melt zone is extremely difficult to maintain in a floating zone growth as sudden flow down of the melt can cause frequent disruption of growth. For melts of such nature, it is more advantageous to contain the melt in a crucible and grow the crystal by a pulling method, such as top-seeded solution growth (TSSG) [21,22].

Here we report the growth of large single crystals of $\text{PbCuTe}_2\text{O}_6$ by both the TSFZ technique in an optical floating zone furnace and TSSG in the high-frequency induction furnace following the Czochralski method. Single crystals grown by these two methods were characterized by powder x-ray diffraction, Laue diffraction, polarized optical microscopy, magnetic susceptibility, and the effects of different growth techniques on the quality of the single crystals are discussed. Finally, by performing heat-capacity measurements down to low temperatures we found a clear λ anomaly at $T \sim 1\text{ K}$ in the single crystals grown by both methods, in contrast to the results for polycrystalline samples. This feature was first discovered and reported in the recent paper, Thurn *et al.* [15]

where it was assigned to a ferroelectric transition accompanied by strong anisotropic distortions by its signatures in a combination of thermal expansion, specific heat, dielectric, and ac susceptibility measurements on the crystals that we describe here. In this current paper, we perform a detailed investigation into the effects of crystallite size, quality, stoichiometry, and show that the transition is an intrinsic property unrelated to impurities or defects, which, however, is suppressed for sufficiently small crystallite size. The origins of this transition and its consequences for the magnetic properties of $\text{PbCuTe}_2\text{O}_6$ are discussed.

II. SAMPLES AND EXPERIMENTAL METHODS

A. TSFZ growth

For crystal growth, first, a polycrystalline powder of $\text{PbCuTe}_2\text{O}_6$ was synthesized by a solid-state reaction of high-purity powder of PbO (99.99%, Alfa Aesar), CuO (99.995%, Alfa Aesar), and TeO_2 (99.9995%, Alfa Aesar) mixed thoroughly in the 1:1:2 molar ratio in ethanol. After mixing, the stoichiometric composition was calcined in a platinum crucible under flowing argon atmosphere in a tube furnace for 12 h at 540°C twice with an intermediate grinding. The powder was then packed into rubber tubes and compressed in a cold hydrostatic press at 2000 bars to form uniform cylindrical rods of length 70–80 mm and diameter around 6 mm. The pressed rods were then hung in the tube furnace and sintered in flowing argon for 12 h at 550°C to form dense rods, ready to be used as the precursor for crystal growth.

Crystal growth was first carried out in an optical floating zone furnace (Crystal Systems Corp., FZ-T 10000-H-VI-VPO) equipped with four 150-W tungsten halide lamps focused by ellipsoidal mirrors. The growths were performed under different atmospheres from 0.1 to 0.2 MPa Argon flow pressure and growth rates ranging from 0.5 to 2.0 mm/h. For crystal growth by the TSFZ technique, we needed to find an optimum solvent, which stays in equilibrium with $\text{PbCuTe}_2\text{O}_6$ when melted. Since no phase equilibrium diagram of PCTO exists, we carefully investigated the reported binary phase diagrams of PbO- TeO_2 , CuO- TeO_2 , and CuO-PbO to get insight into the possible phase relations in the compound [23–25]. Therefore, we constructed the ternary phase diagram of CuO-PbO- TeO_2 as in Fig. 2(a) where the $\text{PbCuTe}_2\text{O}_6$ phase is shown along with the related compounds and their melting temperatures. The blue lines represent the mole fraction of each component of stoichiometric $\text{PbCuTe}_2\text{O}_6$. In addition, thermogravimetry and differential thermal analysis (TG-DTA) were performed on the pure polycrystalline powder of PCTO (NETZSCH TG 209 F3 Taurus) with a heating rate of $5^\circ\text{C}/\text{min}$ over the range of $400\text{--}650^\circ\text{C}$ under Argon flow of 10 cc/min. From the TG-DTA on PCTO, we observe several interesting thermal events [Fig. 2(b)]. We expect that the broad exothermic peak at 556°C corresponds to the decomposition of PCTO, whereas the endothermic peak at 561°C corresponds to the melting of the compound. X-ray powder diffraction shows that the phases after heating to 670°C were $\text{PbCuTe}_2\text{O}_6$, $\text{Pb}_2\text{Te}_3\text{O}_8$, and Cu_3TeO_6 providing further confirmation of the decomposition of PCTO.

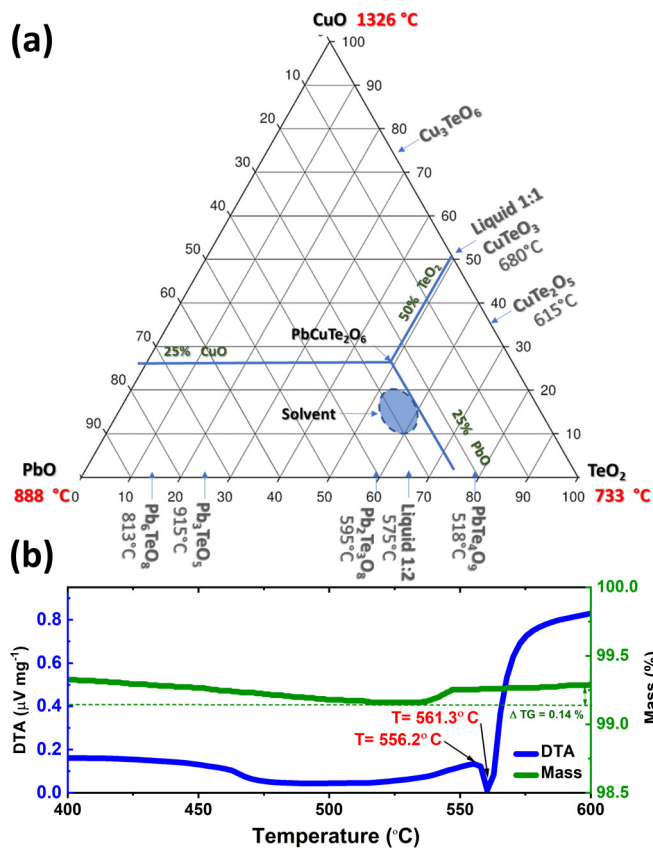


FIG. 2. (a) Ternary phase diagram of $\text{PbCuTe}_2\text{O}_6$ precursors (PbO , CuO , and TeO_2). The blue lines represent the mole fraction of stoichiometric $\text{PbCuTe}_2\text{O}_6$. The blue arrows on the axis represent the stable phases and their melting temperatures. The point of intersection of the blue lines represents the area at which $\text{PbCuTe}_2\text{O}_6$ is expected to form. The dotted blue oval represents the solvent composition for TSFG growth. (b) Thermogram of $\text{PbCuTe}_2\text{O}_6$ powder showing thermogravimetric analysis (TGA) (green line) and DTA (blue line). The broad peak in DTA between 460 and 550°C might be attributed to the melting of small crystallites of PCTO.

Looking into the three binary phase diagrams we conclude that the most probable composition of the solvent with a melting temperature below the PCTO decomposition temperature (556°C) can be found within the blue oval shape shown in Fig. 2(a). For this reason, during the initial experiments, we have used a solvent of composition with excess PbO , TeO_2 . The solvent compound was prepared in the same way as the stoichiometric PCTO by solid-state reactions. Approximately 0.5 g of the solvent was melted and attached to the tip of the stoichiometric feed rod. To begin the crystal growth, only the solvent tip of the rod was remelted and was attached to the seed crystal to form a molten zone.

The DTA technique combined with the TGA is generally used to identify any thermal event related to the sample such as melting, crystallization, decomposition, and structural transition. The melting of any compound is characterized by an endothermic peak in DTA without change in the mass. Although $\text{PbCuTe}_2\text{O}_6$ has an incongruent melting nature, the TG-DTA measurement together with our initial growth experience showed that the incongruent melting temperature of

PCTO is very close to the peritectic point and no mass loss occurred due to evaporation of any other phase, such as PbO . So, it should be possible to grow the PCTO compound without using a nonstoichiometric solvent. For this reason, subsequent growths were carried out just by melting the tip of the stoichiometric feed rod without attaching any off-stoichiometric solvent to it. The growth rate was kept at 1 mm/h allowing the melt composition to change slowly in the next few millimeters to the desired solvent composition that would be in equilibrium with the PCTO phase.

B. TSSG

Top-seeded solution growth of PCTO was carried out in a Czochralski furnace (Mini Czochralski Oxypuller 05-03 Cyberstar, France) equipped with a radio frequency (rf) heating coil and a highly sensitive weighing device attached to the pulling rod to measure growth mass in real time. From our experience of TSFG growth, we found that it was possible to grow PCTO without adding an off-stoichiometric solvent if growth is done at a slow rate. So, a stoichiometric polycrystalline powder of PCTO was prepared as before by solid-state reaction in argon flow. A platinum crucible of 40-mm diameter and 20-mm height was filled with 40 g of well-reacted powder and positioned at the center of the upper part of the coil using a suitable ceramic heating setup. A platinum rod shaped, such as a cylinder of 3-mm diameter and 20-mm length was attached to the pulling shaft to be used as a seed. To minimize the contamination of the chamber, the seed and the powder in the crucible were enclosed in a quartz tube covered by a ceramic lid with a hole to allow the seed movement. The growth chamber was purged and filled with high-purity argon gas a couple of times before heating the coils. The growth was performed under an ambient argon atmosphere with a flow rate of 10 cc/min. The power of the rf heater was increased slowly to 6.5% over 3 h to prevent any evaporation of the precursor. After complete melting, the platinum seed was dipped into the melt and rotated at 5 rpm for mixing. The platinum rod was then pulled upwards at a rate of 0.7 mm/h to initiate the growth from its tip. The growth rate in milligrams/hour was monitored by the highly sensitive weighing device attached to the pulling rod. During the growth, as the amount of the melt in the crucible decreased with time, the diameter of the as-grown crystal was controlled by manipulating the growth speed and the power to the rf coil based on visual observation of the growth and the data obtained from the weighing device. The power of the rf heater was decreased slowly from 6.5 to 6.0%, and the pulling speed was increased from 0.7 to 1.0 mm/h to maintain a stable growth with a mostly constant growth rate of 300 mg/h. The total growth duration was about 72 h resulting in a cylindrical rod of length 65 mm and diameter 4 mm.

The single crystallinity of the crystals grown by both the TSFG and the TSSG methods was checked by x-ray Laue diffraction and polarized optical microscopy (see Fig. 3). Pieces from each crystal were ground and checked with powder x-ray diffraction (PXRD) (Bruker D8) for phase purity. The direct current (DC) magnetic susceptibility χ versus temperature T and isothermal magnetization M versus magnetic-field H measurements were performed using a superconducting quantum interference device (Quantum Design, Inc.).

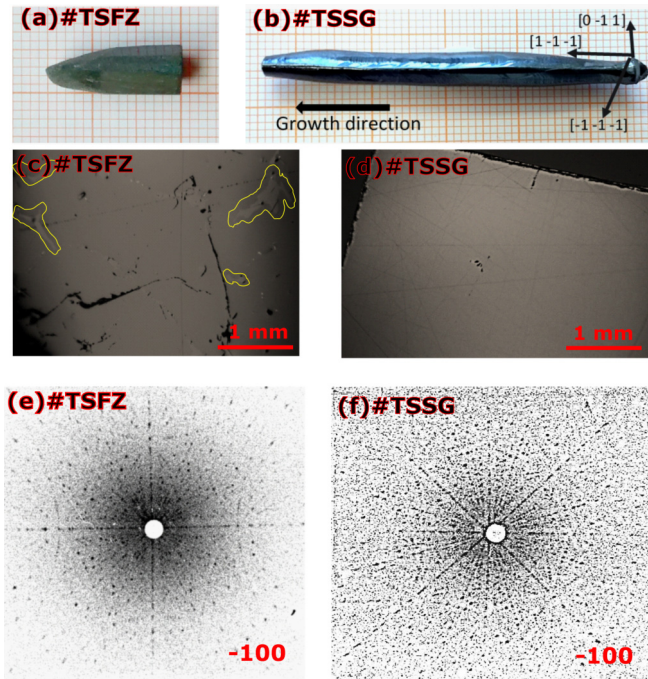


FIG. 3. (a) Representative single crystal of $\text{PbCuTe}_2\text{O}_6$ grown by the optical floating zone method (Crystal TSFZ). (b) Crystal grown by top-seeded solution growth method (Crystal TSSG). (c) and (d) Optical images of the crystal cross section indicating the quality of the TSFZ crystal and TSSG crystal, respectively. The yellow outlines indicate the presence of the impurity phase ($\text{Pb}_2\text{Te}_3\text{O}_8$) in the TSFZ crystal. (e) and (f) Typical x-ray Laue backscattering photographs along the direction $[100]$ of TSFZ and the TSSG crystal.

The temperature dependence of the heat capacity was measured using a physical property measurement system (Quantum Design, Inc.), Measurements down to $T = 0.35$ K were achieved using a ^3He insert. All the growths and characterization measurements were performed at the Core Laboratory for Quantum Materials, Helmholtz Zentrum Berlin.

III. RESULTS AND DISCUSSION

A. Traveling solvent floating zone growth

A single crystal grown by the TSFZ method is shown in Fig. 3(a). The molten zone of growth was observed to be quite unstable. Continuous monitoring was required to maintain the growth because of the low surface tension of the melt, it tends to flow down. This could be attributed to the presence of the heavy metallic elements Pb and Te. The optimum conditions for our growth were found to be at a speed of 1 mm/h in an atmosphere of 0.2 MPa. Growth was performed from a stoichiometric feed rod as the use of a solvent did not seem to have a significant advantage from our experience of previous growths.

The cross section in Fig. 3(c) indicates inclusions (outlined in yellow) in the bulk indicating small amounts of impurities in the single crystal. Nevertheless, the Laue diffraction taken at several points shows clear patterns belonging to the $P4_132$ symmetry of PCTO. Figure 3(e) shows the Laue image with incident x rays along the -100 direction.

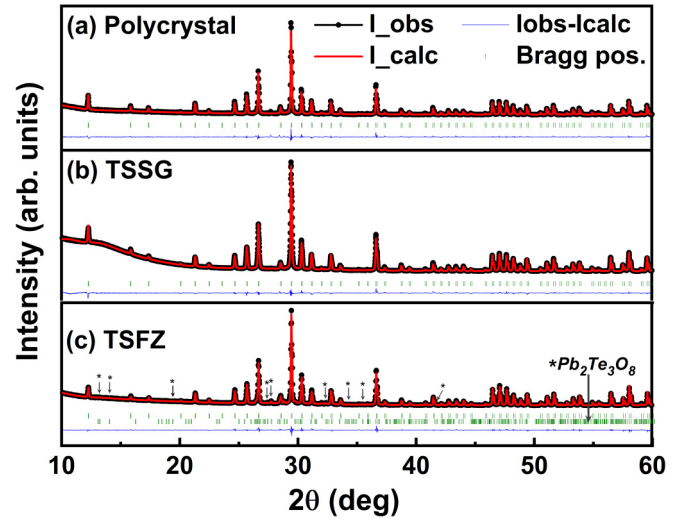


FIG. 4. Comparison of the Rietveld refinement for the powder x-ray diffraction of $\text{PbCuTe}_2\text{O}_6$ crushed samples (a) polycrystalline powder, (b) single-crystal TSSG and (c) single-crystal TSFZ (with $\text{Pb}_2\text{Te}_3\text{O}_8$ additional phase). The solid red line through the experimental points is the Rietveld refinement profile for the $\text{PbCuTe}_2\text{O}_6$ -type cubic structure (space-group $P4_132$). The short green vertical bars mark the Bragg peaks positions, and the lower-most blue curve represents the difference between the experimental and the calculated intensities. The refinement parameters are summarized in Table II. The pronounced background in the TSSG sample is an instrumental error.

B. Top-seeded solution growth

Figure 3(b) shows an as-grown crystal grown by the TSSG method of dimensions of length 65 mm and diameter 4 mm. Unlike the crystal grown by the TSFZ method, TSSG crystal shows nicely developed facets and a shiny surface with a metallic luster. We believe that the different heating techniques as well as the confinement of the powder in a crucible allowed better melting conditions and prevented the melt from flowing downwards as occurred in the TSFZ growth. No inclusion of any impurity phase was found in the cross section of the single crystal as observed by polarized optical microscopy [Fig. 3(d)] or identified by x-ray powder diffraction of crushed crystal from this growth.

X-ray Laue backscattered images taken from both crystals are shown in Figs. 3(e) and 3(f). The TSSG crystal shows considerably sharper Laue photographs, a further testimony of the superior quality of the crystal.

C. Crystallography

The diffraction patterns of polycrystalline as well as a crushed powder from the crystals of PCTO have been measured using x rays ($\lambda = 1.54$ Å) at room temperature. The patterns were refined by the Rietveld method using the FULLPROF software [26]. In all the three samples, the best refinements of the diffraction patterns were obtained by considering a cubic structure of space-group $P4_132$ as shown in Fig. 4. The obtained lattice parameters and the quality parameters of the refinement are listed in Table I. The lattice parameters are 12.498, 12.4967, 12.502 Å for polycrystalline

TABLE I. The Rietveld refinement parameters of $\text{PbCuTe}_2\text{O}_6$ samples including the cell volume (V_{cell}), goodness of fit (GOF) and the R factors: profile R factor (Rp), weighted-profile R factor (Rwp), and expected R factor (R_{exp}). The $(\text{Pb}_2\text{Te}_3\text{O}_8)$ phase present in the TSFZ sample was considered.

Parameter	TSSG	TSFZ	Poly
Lattice parameters	12.49664(24)	12.50196(15)	12.49874(19)
V_{cell} (\AA^3)	1951.5613	1954.043	1952.534
GOF	2.3	0.32	1.7
Rp (%)	2.47	3.19	4.86
Rwp (%)	3.55	4.28	6.30
R_{exp} (%)	1.51	12.89	3.46

(Rwp = 6.30), TSSG (Rwp = 3.55), and TSFZ (Rwp = 4.28) crystals, respectively. These values agree very well with the previously reported polycrystalline $\text{PbCuTe}_2\text{O}_6$ and confirm that the space group is $P4_132$ [8,9]. Allowing the occupancy of the copper ion to vary showed that the refinement favored the stoichiometric sample and did not reveal any disorder of magnetic ion in the $\text{PbCuTe}_2\text{O}_6$ system. A complete list of refined parameters and possible impurities in the samples as well as crystallographic information files are included in the Supplemental Material [27].

Furthermore, the TSSG sample does not show any additional Bragg peaks that do not belong to PCTO, reflecting the single-phase nature of these samples [see Fig. 4(b)]. However, the TSFZ crystal contains some additional Bragg peaks related to the nonmagnetic phase of composition $\text{Pb}_2\text{Te}_3\text{O}_8$ (space-group: $Amam$) as shown in Fig. 4(c) by the stars and lower set of green bars, and Fig. 3(c) indicates the $\text{Pb}_2\text{Te}_3\text{O}_8$ impurity in the microscopy image. This phase has been included in the refinement revealing a phase fraction of 6%. However, we do not see evidence for oxygen deficiency in $\text{PbCuTe}_2\text{O}_6$, which if present, is expected to be less than 0.5%. These values are supported by TGA measurements of different samples of $\text{PbCuTe}_2\text{O}_6$ in oxygen atmosphere which revealed a close to stoichiometric oxygen content (see Supplemental Material [27]).

In a less stable TSFZ growth, 3 to 4% of Cu_3TeO_6 was also observed in addition to the $\text{Pb}_2\text{Te}_3\text{O}_8$ impurity. The presence of both $\text{Pb}_2\text{Te}_3\text{O}_8$ and Cu_3TeO_6 phases in the TSFZ crystal indicated the presence of a eutectic mixture in the growth temperature range.

The microscopic differences in the PXRD patterns of the single crystals TSSG, TSFZ, and polycrystal $\text{PbCuTe}_2\text{O}_6$ are presented in Fig. 4 along with the individual Rietveld refinements to the $P4_132$ structure of PCTO. The fit parameters corresponding to the refinement are listed in Table I. Here, it is clear that both the polycrystal and the TSSG have comparable values of refinement quality, whereas the TSFZ has different values due to the presence of the impurity phase. The presence of the impurity phase in the TSFZ crystal is highlighted and indicated by the additional set of Bragg positions. Finally, we would like to point out that these patterns can also be refined with similar quality by considering the $P4_332$ space group which is the enantiomorphic pair of $P4_132$ used in our analysis.

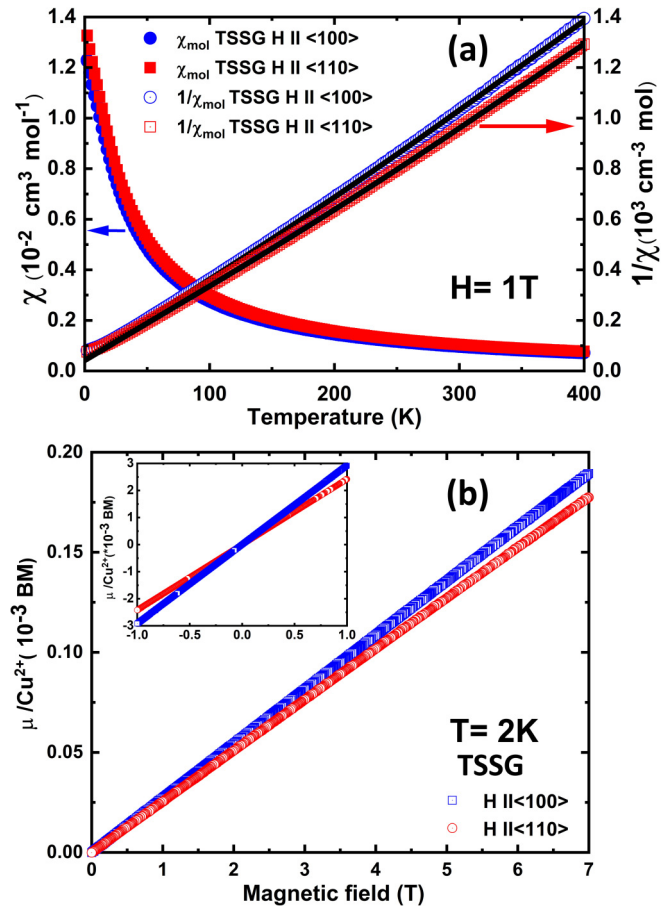


FIG. 5. (a) The temperature dependence of the magnetic susceptibility $\chi(T)$ (left y axis) and $1/\chi$ data (right y axis) of the $\text{PbCuTe}_2\text{O}_6$ TSSG crystal with the magnetic field applied along the [100] and [110] crystallographic directions in the zero-field-cooled condition with a magnetic field of 1 T. The inverse susceptibility data are fitted to the inverse-Curie-Weiss law. (b) Field dependence of the induced magnetic moment along the [110] and [100] directions for the TSSG crystal at 2 K. The inset shows the hysteresis loop at 2 K up to a field range of 1 T.

D. Magnetic properties

Figure 5(a) elucidates the magnetic measurements performed on the two principal directions of the TSSG sample of $\text{PbCuTe}_2\text{O}_6$. The temperature dependence of the molar DC magnetic susceptibility was measured in the temperature range of 2–400 K, using three different applied magnetic fields of 0.1, 0.5, and 1 T. As plotted in Fig. 5(a) for 1 T, the susceptibility revealed a slight anisotropy between [100] and [110] directions at high temperatures in all the measured fields. To quantify these results, the inverse susceptibility data were fitted by the modified Curie-Weiss law considering the total susceptibility, $\chi = \chi_0 + c/(T - \theta_{\text{CW}})$ where c is the Curie constant, θ_{CW} is the Curie-Weiss temperature, and χ_0 is a sum of temperature independent contributions from the core diamagnetism $\chi_{\text{core}} = -1.65 \times 10^{-4} \text{ mol/cm}^3$ and the Van Vleck paramagnetic susceptibility χ_{VV} .

The earlier measurements of inelastic neutron scattering of the single crystal and polycrystalline samples indicated that the magnetic excitation spectrum for PCTO shows only broad

TABLE II. Curie-Weiss fitting parameters obtained from the analysis of magnetic susceptibility of PbCuTe₂O₆ at a field of 1 T.

Sample	$H \parallel$	Range (K)	χ_{vv} (mol cm ³)	Θ_{CW} (K)	(emu K mol)	g factor
TSSG	100	100–300	$7.0(1) * 10^{-5}$	-18.9 ± 0.3	0.34	1.98 ± 0.1
TSSG	110	100–300	$5.6(2) * 10^{-5}$	-18.6 ± 0.3	0.37	1.90 ± 0.1
TSFZ	110	100–300	$8.19(2) * 10^{-5}$	-18.4 ± 0.2	0.43	2.14 ± 0.1
Poly		100–300	$6.7(2) * 10^{-5}$	-20.2 ± 0.2	0.41	2.09 ± 0.1
Reported [9]		20–300	4.5×10^{-5}	-22.0 ± 0.5	0.38	2.0

excitations extending up to 4 meV. This suggests that on the temperature scale, the magnetic correlations could be present up to ~ 45 K. To get a good-quality fitting for paramagnetic susceptibility, we, therefore, varied the lower bound of the fit range above $T_l = 60$ K. The upper bound of the fit was fixed to 300 K for these samples to be compared with the previously reported data on polycrystalline and TSFZ samples [8,9]. For the TSFZ sample, the nonmagnetic impurity Pb₂Te₃O₈ was taken into consideration by normalizing the mass accordingly. The fits were found to be stable for T_l up to 130 K and describe the full range of the linear inverse susceptibility. The resulting fit parameters summarized in Table II for 1 T data suggest a uniform $\theta_{cw} \sim -19$ K for both directions, very close to the previous reports. However, we observe slightly different values of g factor calculated from the fits, namely, $g_{[110]} \sim 2$ and $g_{[100]} \sim 1.9$ indicating that PCTO has a slight deviation from Heisenberg behavior. Possible reasons for the anisotropy could be the Dzyaloshinskii-Moriya interaction which is allowed since the space group is noncentrosymmetric. Another reason could be a single-ion anisotropy of Cu²⁺ due to unquenched orbital momentum. Additionally, anisotropic g factors have also been previously observed in systems where Cu²⁺ sits at the center of plaquettes formed by oxygen ions that are oriented in a preferential direction with respect to crystal axes [28,29]. In PbCuTe₂O₆ too, these plaquettes lie in the six different local [110] planes resulting in a weaker net anisotropy. The effects of weak anisotropy are also visible in the measurements of the isothermal magnetization [see Fig. 5(b)] where the effective moment per Cu ion along the two directions of the single crystal differ as the field increases.

E. Heat capacity

The temperature dependence of the heat capacity of PCTO was investigated for temperature range 0.35–300 K on the polycrystalline and TSSG single-crystal samples.

At high temperatures, i.e., above 2 K the heat capacity of these two samples is very similar and increases smoothly with temperature indicating the phononic behavior. Hence, the lattice contribution was fitted according to the Debye-Einstein (DE) model for $T_l < T < 200$ K using the equation,

$$C_p(T) = \left[9(\text{nat} - C_D - C_{E_i}) R \left(\frac{T}{\theta_D} \right)^3 \int_0^{x_D} \frac{x^4 \exp^x}{(\exp^x - 1)^2} dx \right] + \sum_i C_{E_i} \left[3R \left(\frac{\theta_{E_i}}{T} \right)^2 \frac{(\exp \frac{\theta_{E_i}}{T})}{[(\exp \frac{\theta_{E_i}}{T}) - 1]^2} \right], \quad (1)$$

where nat is the number of atoms per formula, C_D , C_{E_i} are the number of Debye and Einstein modes and θ_D , θ_{E_i} are corresponding temperatures, respectively. The fitting was per-

formed using one Debye term and three Einstein terms, and C_D was fixed to 1. Here, the lower bound T_l was varied between 25 and 50 K in order to accurately extract the magnetic contribution. Figure 6(a) represents the best fit of the DE for the temperature range 28–195 K. The resulting magnetic contribution shows two features for both samples; a peak around 1 K which is sharper for the TSSG sample and a hump at $11.15(\pm 0.04)$ K for TSSG and $10.26(\pm 0.07)$ K for the polycrystal indicating the presence of short-range magnetic correlations (see the inset in Fig. 6). The peak at 1 K is discussed in the next section. The error bars were calculated by fitting the hump with the Gaussian function. The magnetic entropy analysis on the TSSG single crystal and the polycrystalline sample is shown in the inset in Fig. 6(a) in the temperature range 0.35–50 K. The maximum entropy of both TSSG and polycrystal are close to the value expected for a spin $-1/2$ system at 5.76 J/mol ($1 R \ln 2$). Nevertheless, a detailed entropy analysis on the same samples was reported down to 50 mK in another article [15].

On the other hand, the heat capacity of the polycrystalline and single-crystal samples are in stark contrast to each other at low temperatures [see Fig. 6(b)]. The heat capacity of the polycrystalline sample exhibits a second broad anomaly with maxima ~ 1.4 K and then gradually decreases with temperature. However, the heat capacity of the TSSG single crystal exhibits a sharp λ anomaly at 0.98 K indicating a phase transition in the system. Also, the broad maximum under the λ peak occurs at 1.1 K, which is lower than for the polycrystalline sample. Although the λ anomaly is mostly suppressed in the powder samples, in some cases it is observable as a weak peak (see Fig. 7).

F. Low-temperature transition

The λ anomaly in the heat capacity was reported in the recent paper by Thurn *et al.* [15] where it was attributed to a ferroelectric transition accompanied by an anisotropic structural distortion. Here we aim to understand the conditions under which this transition is observed. The difference between polycrystalline and single-crystalline samples could be attributed to two possible origins: first, chemical effects, such as off-stoichiometry, vacancies etc., and second, the sizes of the crystallites in the material.

To test the theory that the discrepancy of the transition at 0.98 K between the single crystal and the polycrystalline samples of PbCuTe₂O₆ is due to the possible nonstoichiometric nature of the as-grown powder samples, two additional polycrystalline samples with excess cation ratios are synthesized. The powders which were synthesized following a similar procedure as explained in the experimental part are

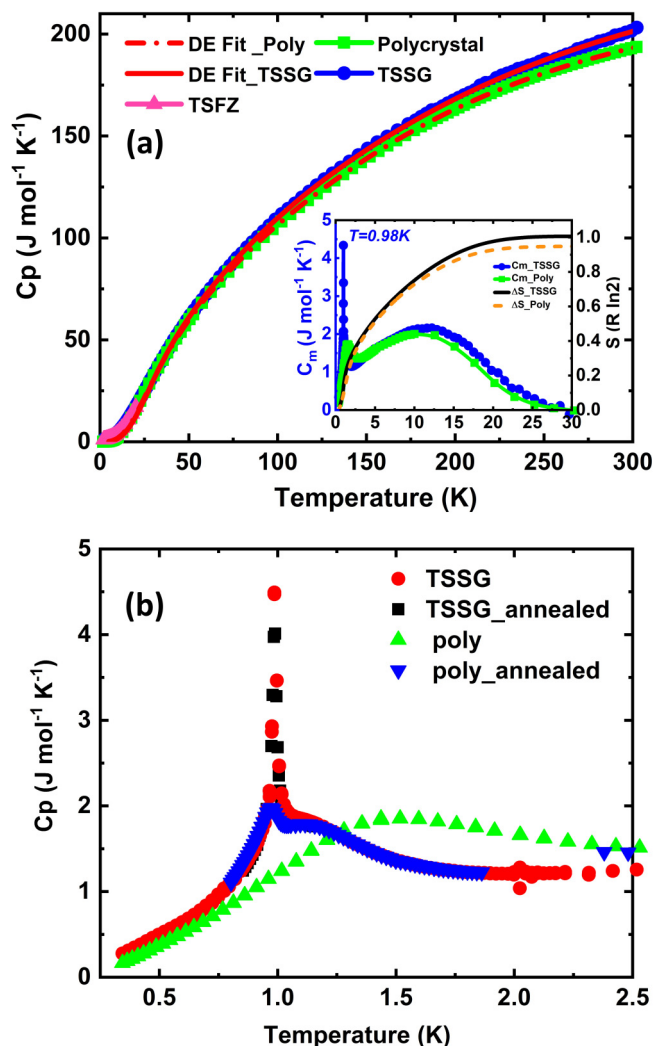


FIG. 6. Temperature dependence of the heat capacity of $\text{PbCuTe}_2\text{O}_6$ in the temperature range 0.3–300 K: (a) Heat capacity of the TSSG, TSFZ, and polycrystal. The red lines represent the fitting of the data according to the Debye-Einstein model for phonon contribution of the heat capacity. The inset represents both the non-phononic heat capacity of the TSSG crystal and the polycrystalline powder extracted by subtracting the phononic contribution (left y axis) and calculation of the change in entropy of both the samples divided by the value $R \ln 2$ (right y axis). (b) Heat capacity of polycrystal and TSSG samples at low temperatures before and after annealing.

$\text{Pb}_{1.02}\text{Cu}_{0.98}\text{Te}_2\text{O}_6$ and $\text{Pb}_{0.98}\text{Cu}_{1.02}\text{Te}_2\text{O}_6$ leading to 2% excess Pb^{2+} or Cu^{2+} in the system. The resulting powders were characterized by obtaining x-ray diffraction patterns at room temperature. We observe that the nuclear structure of the main phase $\text{PbCuTe}_2\text{O}_6$ and the corresponding intensities of the Bragg peaks in the diffraction pattern are unaffected compared to its stoichiometric counterpart. However, peaks corresponding to PbO and PbTe_2O_5 appeared in the excess Pb sample (see the Supplemental Material [27]). For the excess Cu sample, extra peaks attributed to CuTe_2O_5 appeared.

The heat capacity of these powders, plotted in Fig. 7 (with green dots: excess PbO , with red dots: excess CuO) reveals

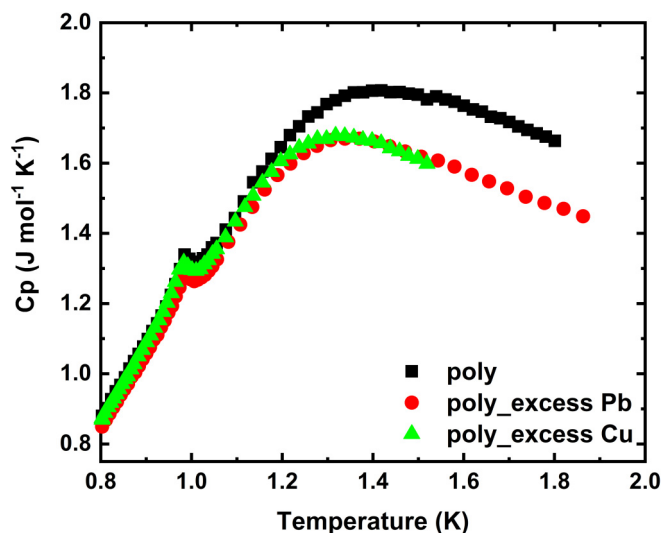


FIG. 7. Comparison of the heat capacity of the $\text{PbCuTe}_2\text{O}_6$ polycrystal with other polycrystalline stoichiometries (2% excess of Pb and Cu).

that the weak transition anomaly at 0.98 K is unaffected suggesting that the stoichiometry of the formed powders is stable, i.e., powders do not suffer off-stoichiometry issues with respect to the cation sites and occupancy which was also confirmed by Rietveld refinement of the PXRD. We also found no evidence for oxygen deficiency in any of the samples. The oxygen content was measured using TGA where the powders were heated in an oxygen atmosphere. As a result, $\text{PbCuTe}_2\text{O}_6$ is oxidized to $\text{PbCuTe}_2\text{O}_7$, and the change in oxygen content is determined from the percentage change in mass. The theoretical value of the change would be 2.57% if the powder before heating had ideal oxygen stoichiometry. TGA measurements showed that the experimental values were close to the theoretical value (see the Supplemental Material [27]) and 0.1% is the tolerance of the oxygen content in both polycrystalline and TSSG samples.

To investigate the theory that the size of the crystallites is responsible for the discrepancy of the transition at 0.98 K between the single-crystal and the polycrystalline samples of $\text{PbCuTe}_2\text{O}_6$ changes in the heat capacity were investigated after crushing the samples to reduce the crystallite size and after annealing them to increase the crystallite size and reduce dislocations and grain boundaries. Figure 8(a) shows similar heat capacity for two different batches of polycrystalline samples (poly_old_as grown, poly_new) synthesized in the same procedure and with starting grain size of approximately $40 \mu\text{m}$. In the next step, one of the powders (poly_old_as grown) was first crushed to a powder of maximum grain size $40 \mu\text{m}$ and then, subsequently, annealed at 525°C for 5 days (grain size after annealing $15\text{--}40 \mu\text{m}$). Although the overall heat capacity is reduced by the smaller crystallites due to crushing, annealing reveals features similar to those observed in the TSSG sample with a sharp peak at 0.98 K and the broad underlying peak at 1.1 K. This suggests that the improved crystallinity and/or increased crystallite size due to annealing leads to the appearance of the transition in the polycrystalline sample.

On the other hand, as shown in Fig. 8(b), the transition anomaly is weakened drastically upon crushing the single

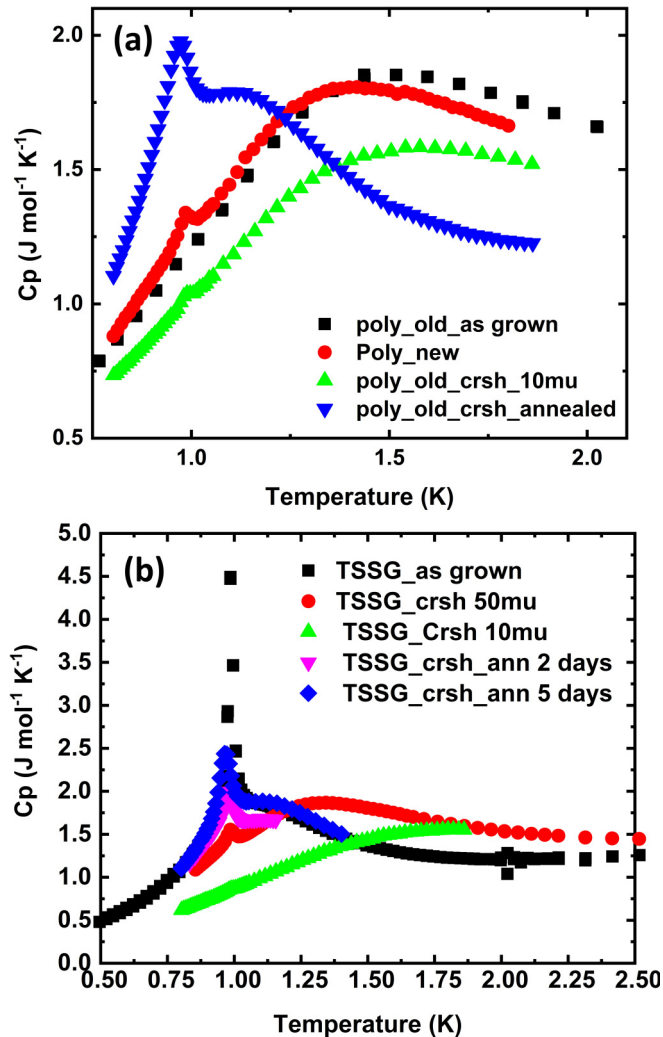


FIG. 8. Size dependence and the effect of annealing on the heat capacity of (a) polycrystal and (b) TSSG samples at low temperatures.

crystal (TSSG) into a fine powder containing crystallites of diameter $30\ \mu\text{m}$ (red circles). The anomaly almost vanishes when the crystallite size is further reduced (maximum diameter $10\ \mu\text{m}$) and the heat capacity (blue triangles) resembles that of the polycrystalline powder revealing the strong influence of the crystallite size in addition to the crystallinity. This is further confirmed when the transition is recovered to a great extent by annealing these crushed crystals which improve crystallite size as well as the crystallinity within the crystallites (grain size after annealing $26\text{--}50\ \mu\text{m}$). Consequently, the longer annealed powder (magenta diamonds, 5 days) exhibits a stronger anomaly compared to the shorter annealing time (green triangles, 2 days).

The transition at 1 K is inherent to the PCTO system, however, it is strongly influenced by the size and crystallinity of the crystallites. As shown in Fig. 6(b), the single crystal shows the sharpest transition whereas a weaker yet distinctive anomaly is found in the annealed powders which is almost absent in the smaller crystallites with poor crystallinity (Fig. 8). A similar scenario has been suggested for a first-order structural transition whose width of the hysteresis is inversely

proportional to the crystallite size [30]. However, the pure structural origin of the transition in the case of $\text{PbCuTe}_2\text{O}_6$ is less likely due to the low temperatures involved. On the other hand, the dielectric anomaly indicating the ferroelectric transition also appears only in the samples with bigger crystallite size (i.e., single crystals) [15]. Therefore it is plausible that the transition is a second-order ferroelastic transition accompanied by a structural transition below which cubic structure breaks into lower symmetry (e.g., tetragonal or orthorhombic) twin domains. In this case, both the ferroelectric as well as a structural anomaly at 0.98 K are absent when the crystallite size is smaller than a critical domain size as has been observed in prototypical ferroelectric materials [31–33].

IV. SUMMARY AND CONCLUSIONS

To summarize, single crystals of $\text{PbCuTe}_2\text{O}_6$ were grown using both TSSG and TSFZ techniques. The challenges in obtaining a pure phase were solved by analyzing the phase diagram and thermal properties of the compound. The difficulty faced in the TSFZ technique to maintain a stable melt zone for a prolonged time could be bypassed using the TSSG technique and higher-quality, large, and impurity-free single crystals could be grown. Both the single crystals and the polycrystalline samples were analyzed using powder x-ray diffraction, magnetic, and heat-capacity measurements. Single crystals revealed an anomaly in the heat capacity around 0.98 K which is nearly absent or much smaller in the polycrystalline samples. The crystallite size of the powders in $\text{PbCuTe}_2\text{O}_6$ play a strong role in the appearance of the transition. The sharp λ peak which was previously shown to be due to ferroelectric order [15] is accompanied by a structural transition in PCTO below which domains are formed due to twinning as a result of symmetry lowering, e.g., from the cubic to tetragonal or cubic to orthorhombic. The transition is intrinsic to PCTO and its suppression in fine-powder samples is unrelated to differences in sample quality or impurities but is rather due to a higher-energy cost of ferroelectric domain formation within small crystallites.

The magnetic properties of PCTO could be affected by the structural transition which would probably alter the bond lengths of the first and second nearest-neighbor $\text{Cu}^{2+}\text{--Cu}^{2+}$ distances making the corresponding interaction strengths different from each other and maybe also splitting each interaction into several inequivalent interactions. This scenario is expected to alter the degree of frustration in the low-temperature phase. In case the frustration is lowered allowing magnetic order to occur, the expected ordered moment will be very small as the spectral weight of the excitations is lowered below $\sim 0.4\ \text{meV}$ at lower temperature [8]. When compared to the simulated diffraction magnetic Bragg peak and the energy scale of the spin waves in the isostructural unfrustrated compound $\text{SrCuTe}_2\text{O}_6$ which develops long-range magnetic order ($1.25\ \text{meV}$) [34,35], the ordered moment in PCTO can be estimated to be less than $0.1\ \mu_B$. It should, however, be noted that the magnetic measurement of Thurn *et al.* [15] do not find an accompanying magnetic transition, rather suggesting that the highly frustrated state survives in the single crystal below the transition with enhanced quantum critical behavior compared to the powders. Therefore, further measurements

focusing on the low-temperature crystal structure and magnetic properties are required to determine the ground state of $\text{PbCuTe}_2\text{O}_6$.

ACKNOWLEDGMENTS

We thank C. Thurn, P. Eibisch, A. Ata, U. Tutsch, Y. Saito, S. Hartmann, J. Zimmermann, B. Wolf, and M. Lang

[Goethe-Universität Frankfurt (M)] who first discover the $T = 1\text{-K}$ transition in $\text{PbCuTe}_2\text{O}_6$ and who supported us with helpful insights into the origins of this feature. This work was supported by the Deutsche Forschungsgemeinschaft (DFG) through Project B06 of the SFB-1143 (Project No. 247310070). The powder synthesis, crystal growth and physical properties measurements took place at the Core Laboratory Quantum Materials, Helmholtz Zentrum Berlin für Materialien und Energie, Germany.

- [1] L. Balents, *Nature (London)* **464**, 199 (2010).
- [2] T. Fennell, P. P. Deen, A. R. Wildes, K. Schmalzl, D. Prabhakaran, A. T. Boothroyd, R. J. Aldus, D. F. McMorrow, and S. T. Bramwell, *Science* **326**, 415 (2009).
- [3] O. Derzhko, J. Richter, and M. Maksymenko, *Int. J. Mod. Phys. B* **29**, 1530007 (2015).
- [4] Y. Zhou, K. Kanoda, and T.-K. Ng, *Rev. Mod. Phys.* **89**, 025003 (2017).
- [5] D. J. P. Morris, D. A. Tennant, S. A. Grigera, B. Klemke, C. Castelnovo, R. Moessner, C. Czternasty, M. Meissner, K. C. Rule, J.-U. Hoffmann, K. Kiefer, S. Gerischer, D. Slobinsky, and R. S. Perry, *Science* **326**, 411 (2009).
- [6] O. Benton, O. Sikora, and N. Shannon, *Phys. Rev. B* **86**, 075154 (2012).
- [7] L. Savary and L. Balents, *Rep. Prog. Phys.* **80**, 016502 (2016).
- [8] S. Chillal, Y. Iqbal, H. O. Jeschke, J. A. Rodriguez-Rivera, R. Bewley, P. Manuel, D. Khalyavin, P. Steffens, R. Thomale, A. T. M. N. Islam, J. Reuther, and B. Lake, *Nat. Commun.* **11**, 2348 (2020).
- [9] B. Koteswararao, R. Kumar, P. Khuntia, S. Bhowal, S. K. Panda, M. R. Rahman, A. V. Mahajan, I. Dasgupta, M. Baenitz, K. H. Kim, and F. C. Chou, *Phys. Rev. B* **90**, 035141 (2014).
- [10] P. Khuntia, F. Bert, P. Mendels, B. Koteswararao, A. V. Mahajan, M. Baenitz, F. C. Chou, C. Baines, A. Amato, and Y. Furukawa, *Phys. Rev. Lett.* **116**, 107203 (2016).
- [11] T.-H. Han, J. S. Helton, S. Chu, D. G. Nocera, J. A. Rodriguez-Rivera, C. Broholm, and Y. S. Lee, *Nature (London)* **492**, 406 (2012).
- [12] C. Balz, B. Lake, J. Reuther, H. Luetkens, R. Schönemann, T. Herrmannsdörfer, Y. Singh, A. T. M. Nazmul Islam, E. M. Wheeler, J. A. Rodriguez-Rivera, T. Guidi, G. G. Simeoni, C. Baines, and H. Ryll, *Nat. Phys.* **12**, 942 (2016).
- [13] M. Weil, M. Shir Khanlou, and T. Stürzer, *Z. Anorg. Allg. Chem.* **645**, 347 (2019).
- [14] L. Wulff and Hk. Müller-Buschbaum, *Zeitschrift für Naturforschung B* **52**, 1341 (1997).
- [15] C. Thurn, P. Eibisch, A. Ata, U. Tutsch, Y. Saito, S. Hartmann, J. Zimmermann, A. R. N. Hanna, A. T. M. N. Islam, S. Chillal, B. Lake, B. Wolf, and M. Lang, [arXiv:2103.17175](https://arxiv.org/abs/2103.17175).
- [16] J. Yeon, S.-H. Kim, M. A. Hayward, and P. S. Halasyamani, *ChemInform* **42** (2011).
- [17] S. Koohpayeh, D. Fort, and J. Abell, *Prog. Cryst. Growth Charact. Mater.* **54**, 121 (2008).
- [18] A. T. M. N. Islam, O. Pieper, B. Lake, and K. Siemensmeyer, *Cryst. Growth Des.* **11**, 154 (2011).
- [19] S. Toth, B. Lake, S. A. J. Kimber, O. Pieper, M. Reehuis, A. T. M. N. Islam, O. Zaharko, C. Ritter, A. H. Hill, H. Ryll, K. Kiefer, D. N. Argyriou, and A. J. Williams, *Phys. Rev. B* **84**, 054452 (2011).
- [20] V. K. Anand, L. Opherden, J. Xu, D. T. Adroja, A. T. M. N. Islam, T. Herrmannsdörfer, J. Hornung, R. Schönemann, M. Uhlarz, H. C. Walker, N. Casati, and B. Lake, *Phys. Rev. B* **94**, 144415 (2016).
- [21] K. Polgár, A. Péter, L. Kovács, G. Corradi, and Z. Szaller, *J. Cryst. Growth* **177**, 211 (1997).
- [22] S. Dagdale, V. Pahurkar, and G. Muley, *Macromol. Symp.* **362**, 139 (2016).
- [23] D. S. Robertson, N. Shaw, and I. M. Young, *J. Phys. D* **9**, 1257 (1976).
- [24] D. Stavrokeva, Y. Ivanova, and Y. Pyrov, *J. Mater. Sci.* **25**, 2175 (1990).
- [25] M. Martínón-Torres, N. Thomas, T. Rehren, and A. Mongiatti, *Archéo Sciences* **32**, 59 (2008).
- [26] J. Rodríguez-Carvajal, *Phys. B: Condens. Matter* **192**, 55 (1993).
- [27] See Supplemental Material at <http://link.aps.org/supplemental/10.1103/PhysRevMaterials.5.113401> for crystal structure refinement details of all the samples reported here.
- [28] S. A. Zvyagin, J. Wosnitza, J. Krzystek, R. Stern, M. Jaime, Y. Sasago, and K. Uchinokura, *Phys. Rev. B* **73**, 094446 (2006).
- [29] E. S. Klyushina, A. C. Tiegel, B. Fauseweh, A. T. M. N. Islam, J. T. Park, B. Klemke, A. Honecker, G. S. Uhrig, S. R. Manmana, and B. Lake, *Phys. Rev. B* **93**, 241109(R) (2016).
- [30] C. Stavrakas, S. J. Zelewski, K. Frohna, E. P. Booker, K. Galkowski, K. Ji, E. Ruggeri, S. Mackowski, R. Kudrawiec, P. Plochocka, and S. D. Stranks, *Adv. Energy Mater.* **9**, 1901883 (2019).
- [31] K. Ishikawa, K. Yoshikawa, and N. Okada, *Phys. Rev. B* **37**, 5852 (1988).
- [32] G. Arlt, *J. Mater. Sci.* **25**, 2655 (1990).
- [33] S. Chattopadhyay, P. Ayyub, V. R. Palkar, and M. Multani, *Phys. Rev. B* **52**, 13177 (1995).
- [34] S. Chillal, A. T. M. N. Islam, P. Steffens, R. Bewley, and B. Lake, *Phys. Rev. B* **104**, 144402 (2021).
- [35] S. Chillal, A. T. M. N. Islam, H. Luetkens, E. Canévet, Y. Skourski, D. Khalyavin, and B. Lake, *Phys. Rev. B* **102**, 224424 (2020).